Fibers and Polymers 2018, Vol.19, No.11, 2254-2267
DOI 10.1007/s12221-018-8027-0

ISSN 1229-9197 (print version)
ISSN 1875-0052 (electronic version)

Adsorption of Graphene Oxide onto Synthetic Fibers: Experimental Conditions

E. Giménez-Martín*, J. A. Moleón-Baca, A. Ontiveros-Ortega, and I. Plaza

Physics Department, University of Jaén, Jaén 23071, Spain

(Received January 14, 2018; Revised August 21, 2018; Accepted August 23, 2018)

Abstract: Comparative studies on the adsorption capacity of two synthetic fibers, polyamide (PA 66) and polyester (PET) pre-treated with N-cetylpyridinium chloride (PET-NCPCl), towards graphene oxide (GO) have been carried out. The fiber samples were characterized by scanning electron microscopy (FE-SEM) and Raman spectroscopy. The results of adsorption isotherms, kinetics, and zeta potential determinations as a function of the GO concentration, pH, and temperature show that at a low pH of 2.5 and a high temperature of 323 K, almost 99 % of the 75 mg/*l* GO solution is adsorbed onto PA 66 and 70 % onto the PET-NCPCl fibers. The interaction should be first attributed to electrostatic forces, also the adsorption data exhibited a good fit to the Freundlich isotherm model and the free energy value of 10 kJ/mol was in the range of physical adsorption, which could suggest that the interaction is driven mainly by physical forces. Due to the increasing development of wastewater treatments based on the GO reactivity with metals and cationic contaminants, synthetic fibers coated with GO could be considered an adsorbent for environmental applications.

Keywords: Adsorption, Synthetic fibers, Graphene oxide, Zeta potential, Kinetic

Introduction

Currently, the increasing amount of polluting substances in surface and ground waters is becoming one of the main problems related to industrial evolution, agriculture practices, and population growth [1-3]. Efforts in many research areas have been made to cope with water pollution, leading to many technological methods, such as photocatalytic oxidation, selective adsorption, flocculation, immobilization, bio-remediation, and biodegradation [4-6]. However, their application presents several problems, such as high energy requirements, difficult operational methods, and low economic benefits. Among the different methods cited to remove contaminants from water, adsorption is the most widely used because of its economic advantages and huge variety of applications [7,8].

Adsorption is particularly suitable because there are many different adsorbent materials depending on the adsorbate that must be linked, with activated carbon being one of the best-known and best-studied adsorbent materials [9-13]. Additionally, the use of nanomaterials (NMs) based on activated carbon, such as graphene [14-16] and iron oxide [17], has provided new methods to remove contaminants from wastewater.

Currently, some of the most studied adsorbents are graphene-family nanomaterials (GFNs) because of their adsorptive properties. Graphene oxide (GO) has several functional groups, such as hydroxyl, carboxyl, and epoxy groups, which provide the molecule with a very high negative charge density and hydrophilicity [18,19]. The oxygen functional groups and the ionizable carboxyl groups allow for ion exchange with metal cations, positively charged organic molecules and polymers, and even anionic compounds, depending on the chemical environmental conditions [14,20,21]. Some authors have studied the interaction between graphene in the form of nanocomposites [22-25] or gel [26,27] and textile fabrics, with the aim of providing the fiber with electrical conductivity properties. In addition, many studies have been reported on using GFNs to remove heavy metals, dyes or organic compounds from wastewater effluents [15,16]. However, knowledge on the environmental behavior of the residual products derived from the link between GFNs and contaminants is scarce. Moreover, the toxicity of GFN derivatives or degradation products to aquatic organisms might be considered. Most of these materials are non-renewable or non-biodegradable, and thus, research attention has recently been focused on the environmental behavior of these residual compounds, which are also potential contaminants [28,29]. Several natural fiber-based materials have been studied, but most of these adsorbents can cope only with pollutants with a single surface charge [30]. Therefore, complex adsorbents with different functional groups could help to solve this problem due to their versatility in interacting with different reactive groups.

For this purpose, after being coated with GO particles, a fiber surface with different functional groups, such as polyamide or polyester treated with an amino compound, could be applied as a versatile adsorptive system towards anionic or cationic contaminants, depending on the pH of the medium. Furthermore, the final product, fiber-GO-contaminant, could be easily removed once the adsorption capacity of GO reaches its saturation value. For this reason, our main goal in the present work is to optimize the experimental conditions for the adsorption of GO on two commonly used synthetic fibers with the aim of a further application for environmental purposes as an adsorbent for the industrial wastewater. These fibers are polyamide fibers, PA 66, which display a high adsorbent capacity when the thermodynamic conditions are optimized, and polyester fibers, PET, which needs to be

*Corresponding author: egimenez@ujaen.es

pre-treated with an amino compound, N-cetylpyridinium chloride, NCPCl, in order to interact with GO particles.

The determinations of adsorption, thermodynamic and kinetic parameters as a function of concentration, pH, temperature, and contact time have been evaluated to optimize the adsorption process and elucidate the mechanism of the interaction between the adsorbent and the adsorbate. One of the most abundant water contaminants is derived from the dye industry, as a large number of residual dyes are poured into the effluent water due to improper processing [30,31], thus leading to a serious environmental problem, particularly in emerging markets with a long tradition in the textile industry, such as India and China. For this reason, an experimental kinetic application of the adsorbent PA 66-GO towards two cationic and one reactive dyes is presented to further control the applicability of this system.

Experimental

Materials

Graphene Oxide (GO)

A commercial water dispersion of GO sheets supplied from Graphenea (Donostia, Spain) of a concentration of 4 g/*l* has been used. The raw material, graphite, is chemically processed to obtain monolayer flakes of GO and the dispersion of odorless GO sheets of variable dimensions is yellow-brown in color. The only absorption wavelength is 235 nm, which means that there are no reduced GO molecules with a wavelength of 300 nm. The calibration curve of the GO dispersion in the concentration range that follows Lambert Beer's law is shown in Figure 1.

N-Cetylpyridinium Chloride (NCPCl)

N-Cetylpyridinium chloride is a cationic surfactant supplied from Merck (Madrid, Spain) and used without further purification. The molecular weight is 340 g/mol, and the absorption wavelength is 258 nm.

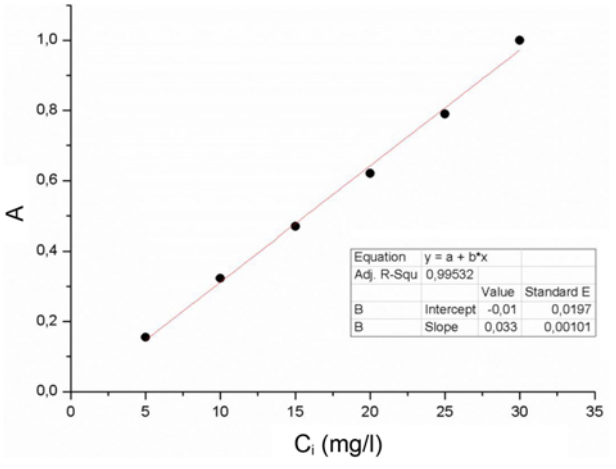

Figure 1. Calibration plot of the GO dispersion.

Fibers

The fiber materials used in this work have been manufactured by Testfabrics, Inc. (West Pittston, PA, USA) and supplied by the Instituto de Investigación Textil y Cooperación Industrial (Terrassa, Spain). The polyamide fibers are 100 % nylon 66 fiber yarn, style 361, with a density of approximately 1.3 g/cm^3 and 1.5 dtex. The molecular weight of the repeating unit is 226.32 g/mol. The polyester fibers are 100 % pure Dacron 54 polyester, with a density of 1.22-1.33 g/cm^3 and 1.3 dtex. The molecular weight of the repeating unit is 192.31 g/mol. The fibers were repeatedly rinsed with deionized water until the supernatant conductivity remained constant, and then they were dried at 313 K in an oven and stored.

Methods

Structural Characterization

The samples of fibers before and after the treatment with a GO solution in the best adsorption conditions were characterized first by Raman spectroscopy with a Raman confocal microscope LEIKA DM LM. The influences of the treatment on the fiber surface morphology were determined by field emission scanning electron microscopy (FE-SEM MERLIN de Carl Zeiss) at an accelerating voltage of 2.5 kV. Elemental analysis of the samples was performed by energy-dispersive X-ray spectroscopy, EDX. The SEM and EDX samples were coated with gold instead of carbon so as not to hide the effect of the carbon atom attributed to the coated GO treatment in the EDX microanalysis. Determinations were conducted at the Center for Scientific and Technical Instrumentation of Jaén University.

Sorption Experiments

Pellets of 1 g of dried fibers were used for sorption and electrokinetic experiments. The samples were dipped in 100 m*l* of GO water dispersion. The influence of the initial concentration in the range of 10 mg/*l* to 75 mg/*l*, the pH of the medium of 2.5 and 4.5, and the temperatures of 293 K, 308 K, and 323 K has been studied. All the batch sorption experiments were performed in a thermostatic water bath (WNB Memmert) with a constant shaking speed and a temperature accuracy of ±0.1 K for 48 h, sufficient time to achieve the equilibrium. The kinetic determinations were performed in the same way. Each experimental determination has been repeated three times, and the average value has been considered for the experimental representations. The amount of the adsorbate that has been uptaken by the fiber was determined from the difference between the initial and final concentrations of the supernatants, estimated by the optical absorbance at 234 nm, with an Agilent Cary 60 UV-Vis spectrophotometer. If the measured sample has an absorbance of over 1 unit, then dilution is needed. However, after the treatment, all the samples exhibited absorbance values below 1, and dilution was necessary only for evaluating the initial concentration of the GO dispersions.

When PET was used as the adsorbent, 1 g of the sample was first conditioned with a 10^{-4} M NCPCl solution at 323 K and pH 6 for 48 hours and then dried in an oven before being used for GO adsorption experiments.

Zeta Potential Measurements

The evolution of zeta potential of the fiber plug has been determined by the streaming potential method, with the Fairbrother-Mastin equation [17]:

$$\zeta = \frac{\Delta U \cdot \eta \cdot K_m}{\Delta p \cdot \varepsilon \cdot \varepsilon_0} \quad (1)$$

where ΔU is the streaming potential, Δp is the pressure difference, K_m is the conductivity of the electrolyte solution; and η is the dynamic viscosity of the electrolyte solution. The zeta potential has been determined by the streaming potential with an Electrokinetic Analyser, EKA (Anton Paar, KG). Samples of 1 g of fibers were placed between two electrodes at a constant distance of 1 cm of a cylindrical cell of 20 mm in diameter, which corresponds to a bulk sample density inside the cell of approximately 0.32 g/cm^3. An electrolyte solution of 10^{-3} M KCl was forced to stream along the solid surface by a pressure difference, and the flow should change its direction periodically. The streaming potential was measured with two Ag/AgCl electrodes placed at both sides of the sample. The data are obtained by the average value of three measurements.

Results and Discussion

Effect of the Initial pH on the Zeta Potential

Figure 2 plots the evolution of zeta potential, ζ, of the three fibers, PA 66, untreated PET, and PET-NCPCl, as a function of the pH of the medium, 10^{-3} M KCl, in the range of 2-10. In the three situations, H^+ and OH^- ions are the determinant ions for the zeta potential. First, it can be observed that in the pH range evaluated, negative values of the zeta potential of PET-NCPCl are always lower than those of untreated PET, as reported previously by us [32]. The isoelectric point, IP, for the PET fibers is approximately pH 2.3, similar to the level determined by various authors [33,34]. If the fiber is treated with 10^{-4} M NCPCl, the IP changes towards a higher value of approximately 4.2 because of the surfactant molecules previously adsorbed on the fiber surface. Both fibers at a pH value lower than 4-4.5 exhibit a positive charge due to the adsorption of H^+ ions from the acid medium in the double layer and the protonation of the amino groups. However, for pH values higher than the IP, the surface is mainly negatively charged because of the ionization of the acid groups and the adsorption of OH^- ions.

In Figure 3, the evolution of zeta potential of PA 66 fibers as a function of the concentration of the GO dispersion at two pH values of 4.5 and 2.5 is presented. A similar study has been performed previously on PET fibers [32]. In both

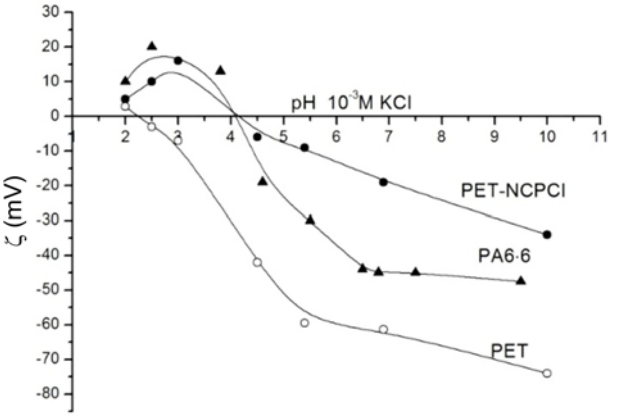

Figure 2. Evolution of zeta potential as function of the pH of KCl 10^{-3} M, for the fibers.

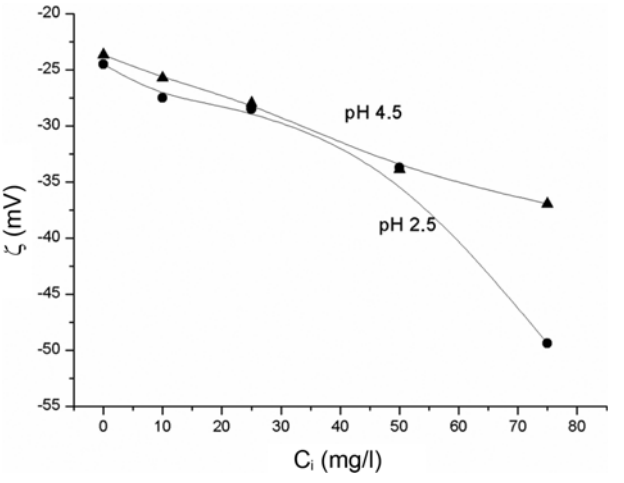

Figure 3. Evolution of zeta potential of PA66 fibers as function of the initial concentration of GO dispersion and the pH of the medium.

situations, the zeta potential increases its negative value with the concentration of the GO dispersion. When the GO concentration is 50 mg/*l*, which has been determined by electrophoretic measurements, the zeta potential is between -30 and -35 mV. No differences with the pH of the dispersion can be found for a GO concentration lower than 75 mg/*l* because at this concentration, a high coverage of the fiber surface by GO particles could be achieved, with its negatively charged groups being responsible for the increase in negative zeta potential values. This effect is more determinant if the adsorption occurs at pH 2.5, where the multilayer deposition could be suggested to explain the high negative zeta potential value.

Table 1 summarizes the values of zeta potential for the untreated fibers and the fibers treated with a 75 mg/*l* GO solution at pH 4.5. An increase in the negative zeta potential of the fiber surface can be observed due to the adsorption of GO particles. In addition, an abrupt diminution of the zeta

Table 1. Zeta potential values of the fibers

Fiber	ζ(mV)
PET	-42.0±2.1
PET-NCPCl	-6±0.3
PA 66	-19±1
PET-NCPCl - 75 mg/*l* GO	-42,7±2.4
PA 66 - 75 mg/*l* GO	-34.5±1.7

potential of PET occurs when the fiber is treated with the cationic surfactant NCPCl, which decreases the negative charge of the untreated PET surface.

Adsorption

The influence of pH on the GO adsorption onto PA 66 at a higher concentration of 75 mg/*l* and a temperature of 323 K is presented in Figure 4. Two regions with different slopes could be observed, the first one from pH 2 to 3.5 where the adsorption capacity experiments show an abrupt decrease with increasing pH, and the second one with a softer negative slope. From the result presented, two pH values have been chosen for our study, pH 2.5, at which the fiber exhibits the maximum adsorption capacity, and pH 4.5, which corresponds to the pH of GO solutions and is the pH of the higher amount adsorbed in the second region. The same pH values have been used for the PET-NCPCl experiments.

Figure 5 presents the average percentage of the adsorption capacity of the two fibers as a function of the pH and temperature of the GO dispersion for a solution with an initial concentration of 75 mg/*l*. It can be observed that there is a marked influence of the pH of the medium on both fiber treatments, and a noticeable decrease in the amount

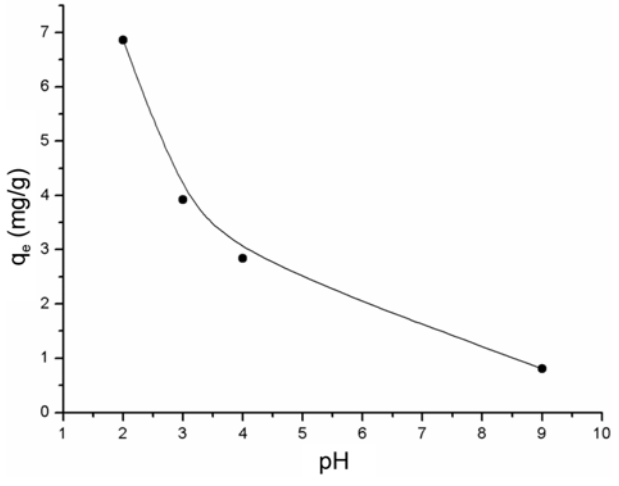

Figure 4. Amount of GO adsorbed onto PA 66 treated with 75 mg/*l* of GO dispersion at 323 K as function of the pH of the medium.

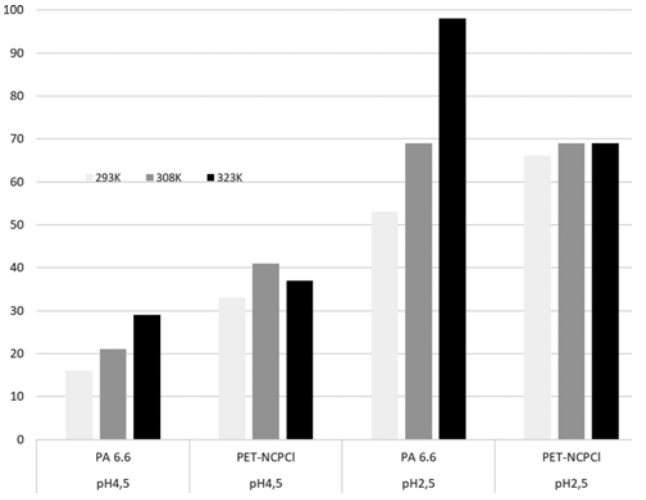

Figure 5. Percentage of adsorption of GO on PA 66 and PET-NCPCl fibers as function of the pH and temperature.

adsorbed is observed when the pH value is 4.5. By contrast, it seems that temperature only affects the adsorption behavior of the PA 66 fibers. The positive effect of both a low pH value of 2.5 and a high temperature of 323 K on the PA 66 fibers is so evident that almost 99 % of the 75 mg/*l* GO solution is adsorbed, and the supernatant solution remains almost clear after the treatment. When the adsorbents are PET-NCPCl fibers, the situation is slightly different and the influence of the temperature on the process is very small. At pH 4.5, which is the less favorable pH for this process, the percentage adsorbed is higher than that for the PA 66 fibers. Regardless of the tested temperature, even though the amount adsorbed at pH 2.5 increases considerably compared with pH 4.5, it does not reach the percentage of adsorption reached by PA 66 (99 %). Nevertheless, the adsorption could still be considered quite effective, obtaining values near 70 %.

Structural Characterization

The surface morphologies of PA 66-GO and PET-NCPCl-GO as well as those of the fibers without the GO treatment were analyzed by FE-SEM and the fiber diameters were also measured, which are presented in Figure 6(a) to 6(d) for the PA 66 fibers and Figure 7(a) to 7(d) for the PET-NCPCl fibers. All the samples are coated with gold instead of carbon to improve the quality of the microphotographs and avoid the interferences with carbon from the GO treatment. Figure 6(b) and 7(b) show a general image of the fibers. A large number of GO sheets are observed covering or wrapping the PA 66 fibers, while for the PET-NCPCl fibers, the molecules are discontinuously clustered and anchored at separate points, possibly where the NCPCl molecules are previously bounded. Figure 6(c) and 6(d) show the fibers' detail. Again, it can be observed that the GO sheets appear to envelop the polymer of PA, suggesting

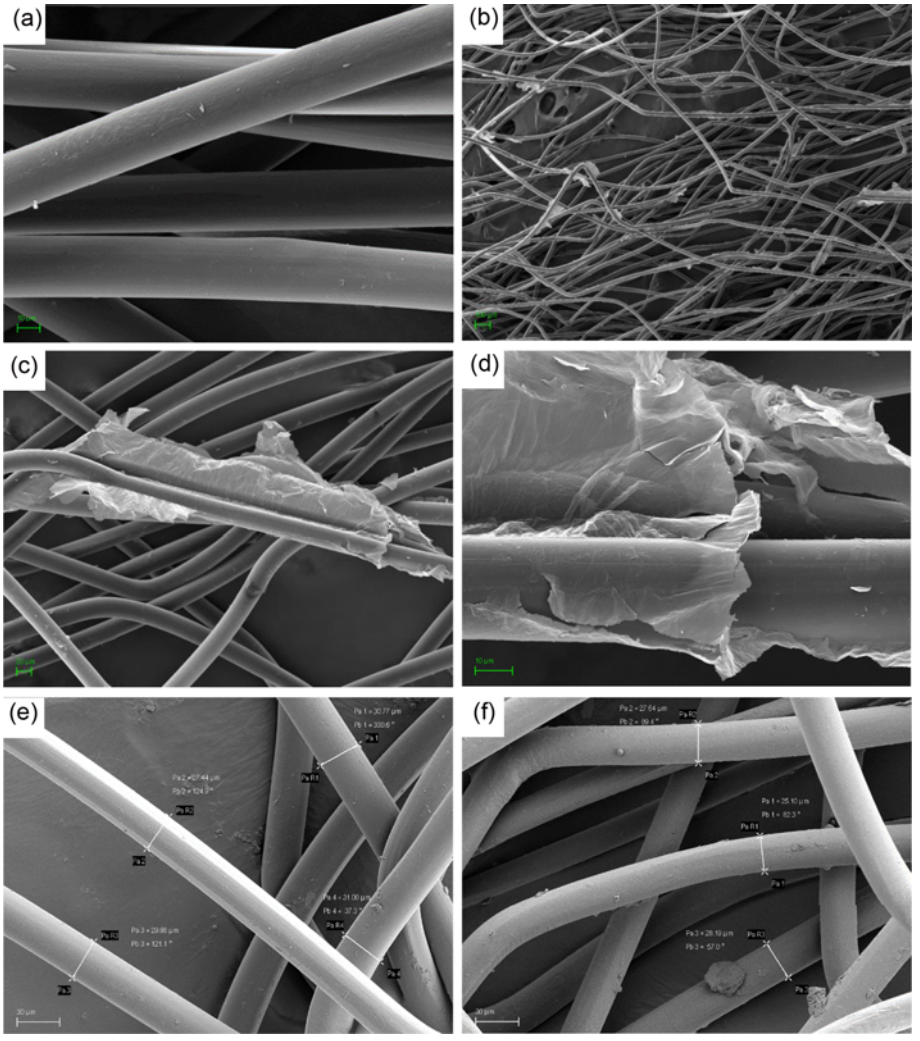

Figure 6. SEM images of PA 66 fibers; (a) untreated 1500×, (b) PA 66-GO 100×, (c) PA 66 500×, (d) PA 66-GO 2500×, (e) untreated PA 66 1000×, and (f) PA 66-GO 1000×.

a certain uniformity in the coating of the fiber, possibly pointing to a monolayer coverage. By contrast, in Figure 7(b) and 7(d), molecular clusters seem to be specially formed, and therefore, a great heterogeneity in the fiber coating is observed, with the GO particles forming agglomerated aggregates or lumps because of the interaction between the GO particles. This formation could result in a multilayer arrangement at the places where the NCPCl molecules were previously linked. Figure 6(e), 7(e), 6(f), and 7(f) present the fiber diameter measurements. Apparently, there is no influence of GO on the PET fiber diameter (11.62 μm for PET-NCPCl and 11.60 μm for PET-NCPCl-GO). By contrast, for the PA 66 fibers, the average diameter diminishes slightly from 29.8 μm to 26.98 μm. In our opinion, this result could be attributed to a higher hydrophilicity of the fibers due to the increasing hydrogen bonding formed between GO and the amino groups of the fibers, which could lead to a narrowing in the space between the polymer chains [35].

Figure 8(a) to 8(f) show the EDX microanalysis of two areas of the untreated (Figure 8(a) and 8(d)) and GO coated fibers, the first, Figure 8(b) and 8(d), over GO aggregations and the second, Figure 8(c) and 8(f), in the same fiber filament but with no GO molecules. A slight increase in the O atom and Au and the presence of Cl in the treated fibers can be highlighted from these results. Cl appears because the acid pH of the treatment is adjusted with HCl, and the increase in the amount of oxygen atoms can be attributed to the GO particles that are composed a high amount of oxygen groups. Additionally, it seems that Au is better fixed to the GO treated fibers, probably because the negative charge of the surface interacts with this cation. However, although image evidence of GO in the photographs is observed, the microanalysis does not provide significant information

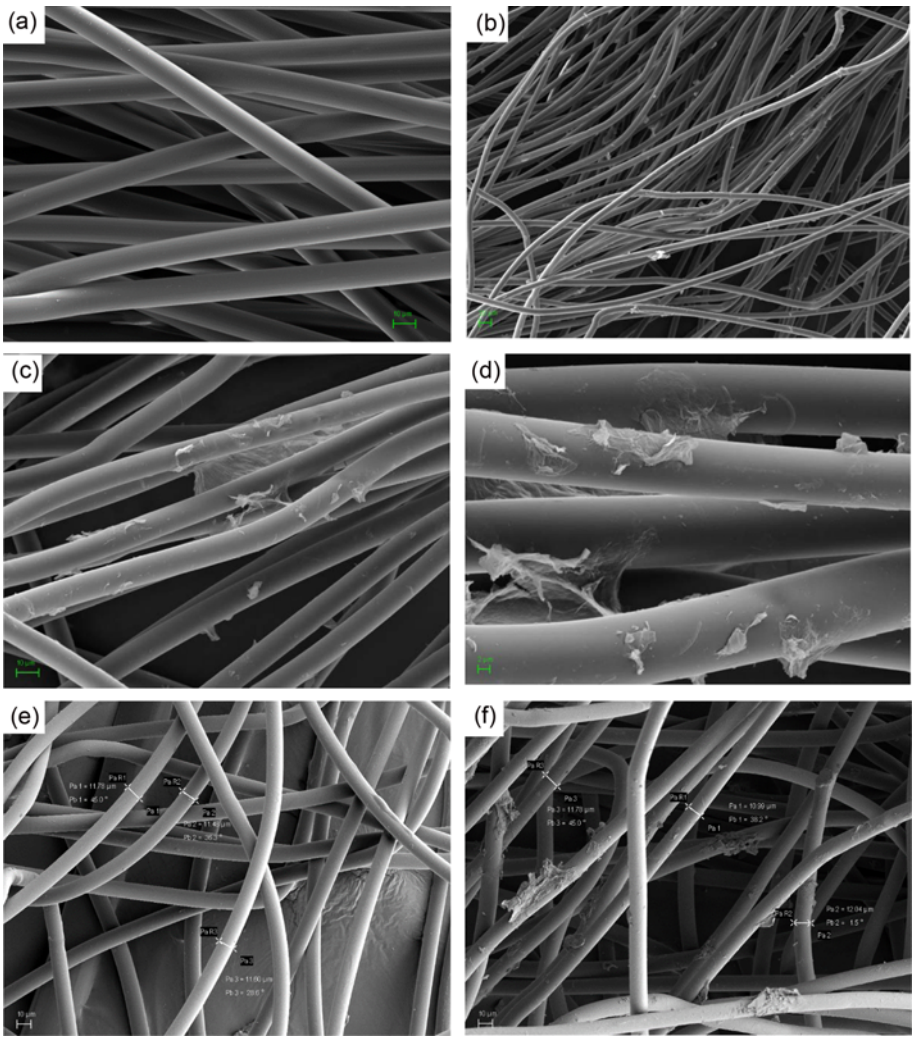

Figure 7. SEM images of PET fibers; (a) untreated 1500×, (b) PET-NCPCl-GO 400×, (c) PET-NCPCl-GO 1500×, (d) PET-NCPCl-GO 2500×, (e) untreated PET 1000×, and (f) PET-NCPCl-GO 1000×.

about the change in the composition.

Comparative Raman spectra for both fibers in Figure 9(a) and 9(b) show the influence of the treatment on the intensity of the representative peaks of the fibers. The intensity of the characteristic peaks of graphene is similar in both fibers. In Figure 9(c), the overlapping of the Raman spectra for both fibers treated with GO is presented. The D band, which is ascribed to no crystalline structure and local disorder [35,36], is located between 1352 and 1354 cm^{-1}, corresponding to the GO particles. The G band, which corresponds to the sp^2 stretching motion of carbon atoms, shifts from 1608 cm^{-1}, corresponding to the bare GO, to 1601 cm^{-1} and 1603 cm^{-1} for PET-NCPCl-GO and PA 66-GO. Similar results were obtained by Ramesha and collaborators [16] when working with different dyes. They suggested that this shift to lower values could be due to the charge transfer that occurs between the adsorbent and the adsorbate when the electrostatic and van der Waals interactions are the driving forces. Consequently, as the shift for PA 66 is higher than that for PET-NCPCl, and at the experimental pH 2.5, the amine groups are protonated, which could suggest that the electrostatic interactions are more important in this situation. Finally, the I_D/I_G ratio is 0.85 for PA 66 and 0.83 for the PET fibers.

Adsorption

The experiments of equilibrium adsorption isotherms at three temperatures and two pH values were performed, and the results obtained for PA 66 and PET-NCPCl are presented in Figure 9 and Figure 10, respectively, where the amount of GO uptaken at the equilibrium, q_e (mg GO/g of fiber), as a function of the equilibrium concentration (mg GO/*l*) is plotted.

In both situations, the adsorption increases with the

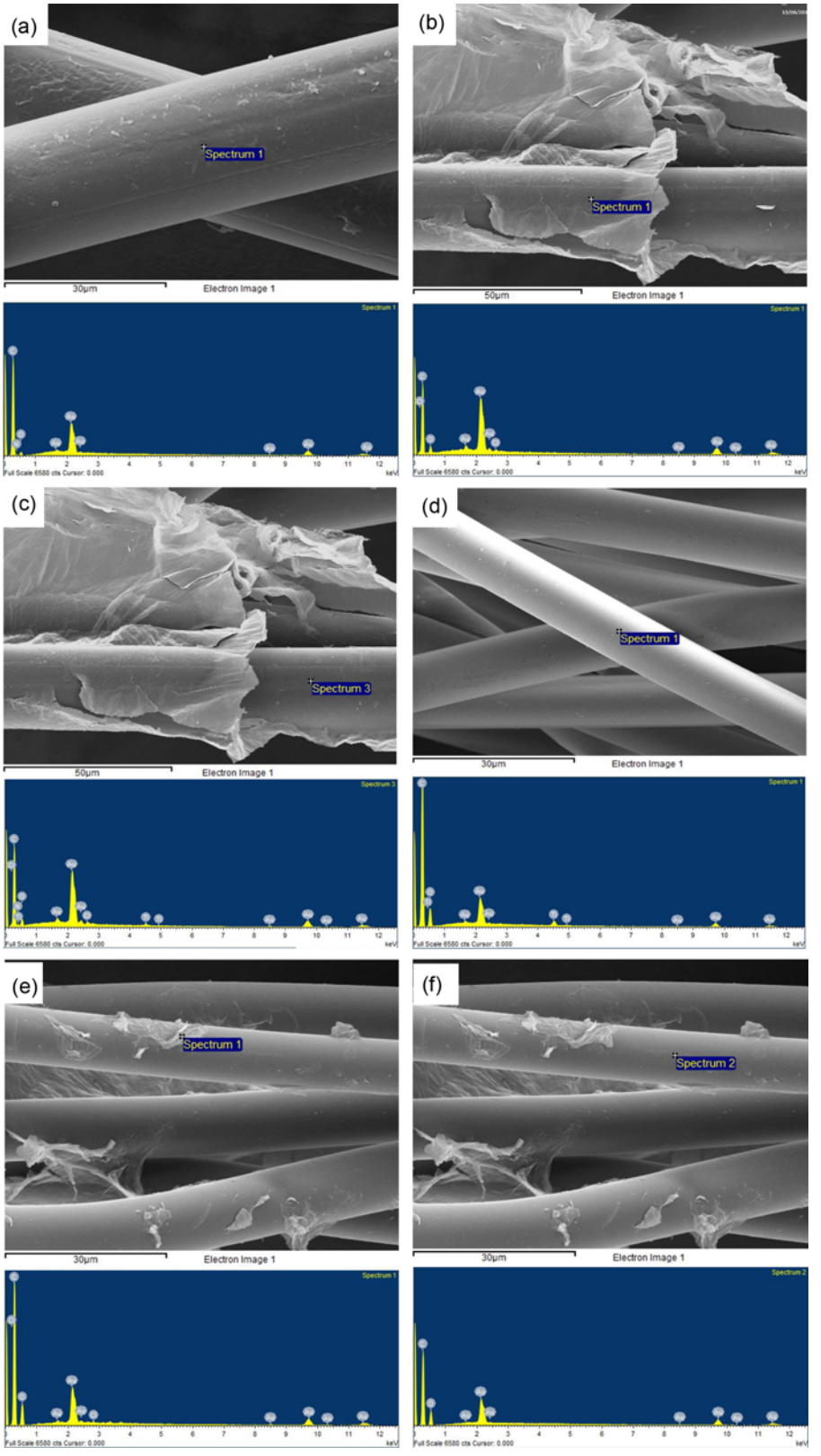

Figure 8. (a) EDX microanalysis of untreated PA 66, (b) EDX microanalysis of PA 66-GO on the GO sheet, (c) EDX microanalysis of PA 66-GO off the GO sheet, (d) EDX microanalysis of untreated PET, (e) EDX microanalysis PET-GO on GO sheet, and (f) EDX microanalysis of PET-GO off the GO sheet.

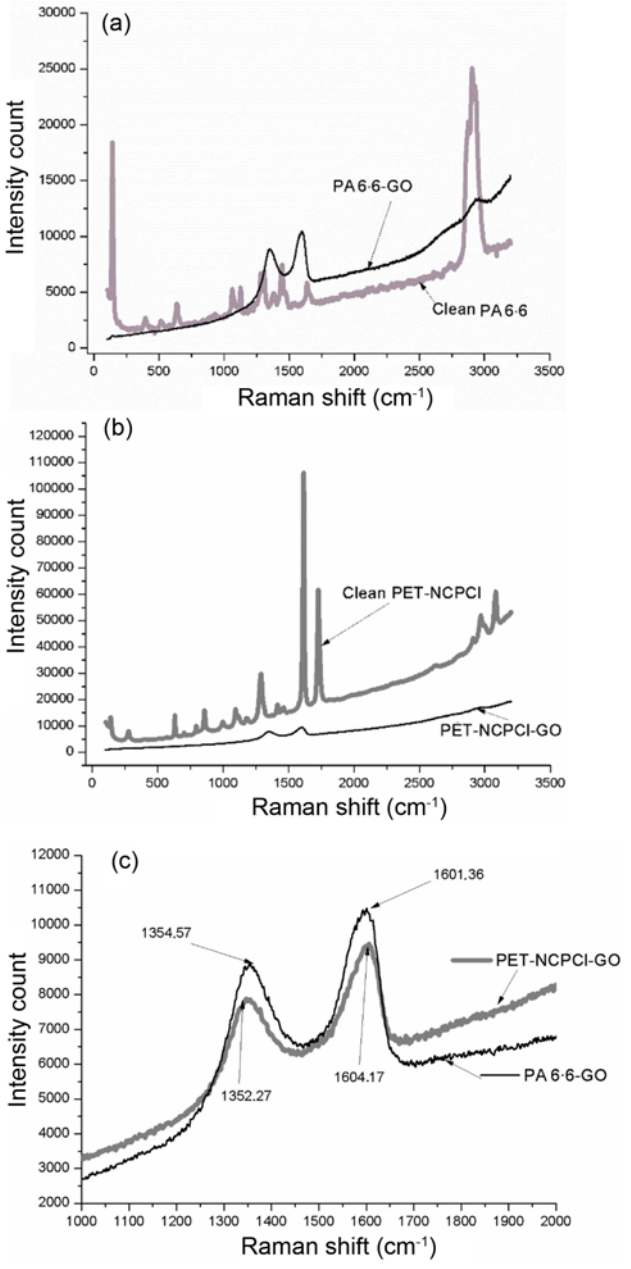

Figure 9. Raman spectra for (a) PA 66, (b) PET, and (c) significant bands of both fibers.

concentration of the GO solution, and it seems that the saturation is not reached at pH 2.5. Although both figures exhibit the same trend, where the adsorption capacity increases at a lower pH value, the effect of temperature at pH 2.5 is quite different. The *S* type isotherm at all the temperatures tested and the lower pH value, where no saturation value is reached, could suggest two steps in the process – first, adsorbent-adsorbate interactions, followed by adsorbate-adsorbate interactions – which could explain that the fibers do not reach a plateau value of saturation at the

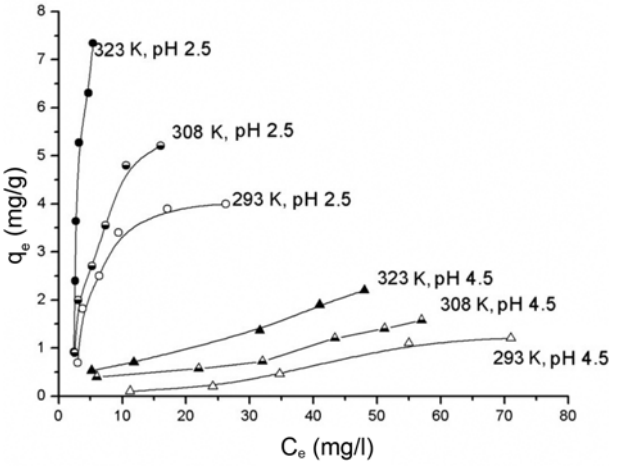

Figure 10. Amount GO adsorbed onto PA 66 fibers as function of the concentration, the temperature and the pH.

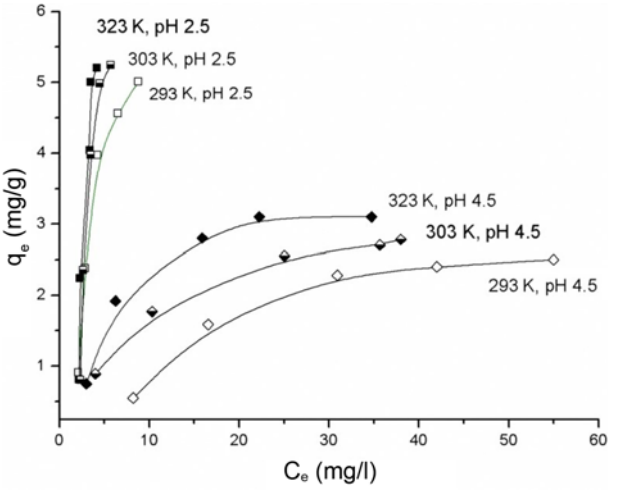

Figure 11. Amount GO adsorbed onto PET-NCPCl fibers as function of the concentration, the temperature and the pH.

higher concentration.

Equilibrium Adsorption Isotherms

The equilibrium adsorption isotherm analysis is essential to describing the interaction behavior in the adsorption process from a water solution onto a solid adsorbent of textile fibers.

Langmuir Isotherm

The Langmuir isotherm model [37] assumes that sorption occurs at specific homogeneous places within the adsorbent where all sorption locations are identical and energetically equivalent and there is no interaction between the molecules adsorbed at neighbouring sites. Therefore, a saturation value is reached beyond which no further sorption can occur. This theory considers that the adsorbent behaves as an ideal solid surface, where the adsorbate can be bonded by either

physisorption or chemisorption. The intermolecular forces decrease abruptly with the distance and the model only predicts a monolayer coverage. The Langmuir model equation is

$$q_e = \frac{X_m a_L C_e}{1 + a_L C_e} \quad (2)$$

where q_e is the equilibrium concentration of the adsorbate per unit weight of the dry adsorbent (mg/g), C_e is the equilibrium concentration of the adsorbate in the solution (mg/*l*), X_m and a_L are Langmuir constants related to the theoretical monolayer capacity (mg/g) and the affinity binding sites (*l*·mg), respectively. The constants have been determined from a linear fit of equation (2) in the following form:

$$\frac{C_e}{q_e} = \frac{1}{X_m a_L} + \frac{1}{X_m} C_e \quad (3)$$

Freundlich Isotherm

This model is the earliest known relationship describing the non-ideal and reverse adsorption, which is not restricted to a monolayer [38], and the empirical model can be applied to the multilayer adsorption on a heterogeneous surface and the adsorbate-adsorbate interactions. The amount adsorbed is the sum of the adsorption at all sites with the stronger binding sites being occupied first, until the adsorption energy exponentially decreases upon the completion of the adsorption process. The empirical equation is

$$q_e = K_F C_e^{1/n_F} \quad (4)$$

where K_F is the Freundlich constant (*l*/mg) and $1/n_F$ is the heterogeneity factor. If $n>1$, then the adsorption is favorable. From a linear fit of equation (4), these empirical values were obtained.

$$\ln q_e = \ln K_F + \frac{1}{n_F} \ln C_e \quad (5)$$

Both equilibrium isotherm models were tested, but both systems could be fitted only to the Freundlich model. These results suggest that the adsorption of GO on these two fibers occurs under a certain kind of unspecific interactions, adsorbate-adsorbate interactions, which lead to increasing adsorbate concentration on the adsorbent and thus, a saturation concentration is not reached, as observed in Figures 8 and 9. This situation is typical for a heterogeneous surface. Similar observations have been presented by different authors working with GO as the adsorbent for metals [18]. Table 2 lists the values for Freundlich constants. It can be observed that the adsorbent capacity of the Freundlich model, K_F, presents higher values at pH 2.5 (although the trend of this parameter with temperature is not clear), and the values of $1/n$, which indicate the adsorption intensity, are generally in the range of 0 to 1, which means that the adsorption conditions are favourable. The wide range of variation in $1/n$ values could reveal the adsorption sites with a broad energy distribution. To explain the slight influence of temperature on the PET-NCPCl/GO adsorption, it could be considered that the main interaction occurs between the GO particles and the pyridine ring of NCPCl ionized at pH 2.5. However, besides this electrostatic interaction (EL), the acid-base interactions (AB), Lifshitz-van der Waals (LW) forces and π-π stacking interactions between the benzene ring of the graphene sheets previously adsorbed and the particles in solution must be considered. This kind of interaction does not depend on the temperature. When the adsorbent is the PA 66 fibers, in our opinion, the main adsorption forces should be the electrostatic interactions between the amine group of the fiber and the negatively charged groups of GO. If the influence of pH is considered, the adsorption capacity at pH 2.5 is very high, and the effect of temperature is important, as it has been described with other systems [39]. This last situation could be attributed to the influence of temperature on the reaction of the protonation of amine groups, and as the reaction is endothermic, an increasing number of the particles may acquire enough energy to undergo an interaction with more energetic sites of the fiber [40]. This effect is more pronounced at pH 2.5 than at pH 4.5, which is near the IP of the fiber, and therefore, the charge is almost zero; hence, the electrostatic interactions should be scarce, and the influence of temperature on the amount adsorbed at pH 4.5 is less important. A similar influence of temperature and pH is observed when dyeing polyamide fibers with acid dyes and reactive dyes [34,41].

Thermodynamic Functions

Thermodynamic studies can reveal important information about the energy changes involved in the adsorption process. The standard free energy of adsorption, ΔG^o at a temperature *T*, can be evaluated from the following equation assuming the ideal behavior of the solution:

$$(\Delta G^{\circ})_T = -RT \ln K_c \quad (6)$$

where the term $[(q_e/V)/C] = K_c$ is the process constant, in which *V* is the specific volume of the fiber (0.87-1.15 *l*/kg). The data obtained from the bibliography and the experimental determinations have been assumed to be 1 *l*/kg [34,42].

The standard enthalpy change ΔH° and the standard entropy change ΔS° of the adsorption can be estimated by fitting $\ln K_c$ against $1/T$ using the following equation:

$$\ln K_c = -\frac{\Delta H^{\circ}}{RT} + \frac{\Delta S^{\circ}}{R} \quad (7)$$

The values obtained from the fitting of the experimental data to equations (6) and (7) are shown in Table 3. The negative values of Gibbs free energy at pH 2.5 and 323 K point to a spontaneous adsorption only under these

Table 2. Freundlich constant values for adsorption of GO over the PA 66 and PET-NCPCl fibers as function of pH and temperature

pH	Freundlich constants	323 K		308 K		293 K	
		PA 66	PET-NCPCl	PA 66	PET-NCPCl	PA 66	PET-NCPCl
2.5	K_F (mg/g)	1.617	0.958	1.016	0.718	1.153	2.507
		1.009	0.967	1.625	0.691	2.417	3.125
		1	1.034	0.615	1.449	0.414	0.321
		0.9	0.7	0.98	0.82	0.91	0.998
4.5	K_F (mg/g)	0.094	0.491	0.016	1.157	0.003	1.316
	n	1.247	2.036	0.888	3.355	0.686	6.255
	1/n	0.802	0.491	1.112	0.298	1.458	0.159
	(R^2)	0.96	0.9	0.94	0.74	0.94	0.996

Table 3. Thermodynamic parameters

Fiber	pH	ΔH^o (kJ/mol)	ΔS^o (J/ mol·K)	ΔG^o (kJ/mol)		
				293 K	308 K	323 K
PA 66	pH 2.5	+59.29	+184.75	+5.68	+2.63	-0.132
	pH 4.5	+27.15	+58.28	+10.15	+8.97	8.09
PET-NCPCl	pH 2.5	+20.29	+64.63	+1.54	+0.38	-0.58
	pH 4.5	+23.32	+52.37	+7.68	+6.88	+6.06

conditions [43]. It can be observed that all the processes are endothermic, with the value of enthalpy change being higher for the PA 66 fibers at both pH values, pointing to a higher influence of temperature, as observed previously in the isotherm graphics (Figure 8). The positive value of entropy change might correspond to an increase in the degree of freedom of the adsorbed species [39], with this value being greater for PA 66 at pH 2.5, possibly because the amount of GO particles adsorbed is the higher one.

Kinetics of Adsorption

The interpretation of the adsorption kinetic data allows us to estimate the adsorption rate, and their fitting to different kinetic empirical models is necessary to evaluate the mechanism of the adsorption of solute onto the adsorbent. These experimental data, at different temperatures and pH values, are plotted in Figure 11 and Figure 12 for the two fibers, respectively.

The experimental kinetic data were fitted to the pseudo-first-order [44] and pseudo-second-order models [45]. The pseudo-first-order model describes the adsorption of a liquid/solid system based on the solid capacity, with the following equation:

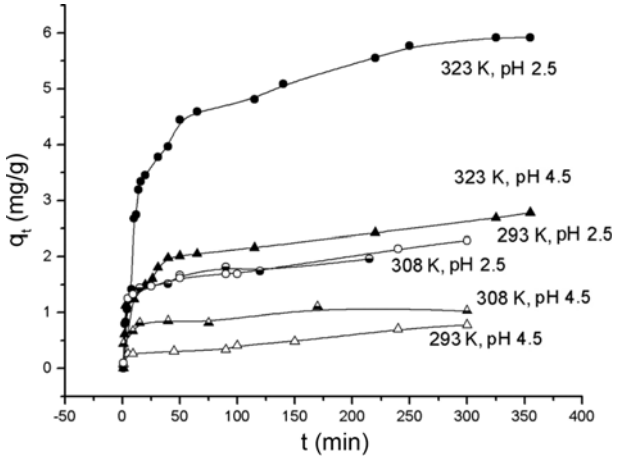

Figure 12. Kinetic adsorption isotherms of PA 66 fibers as function of the pH and the temperature.

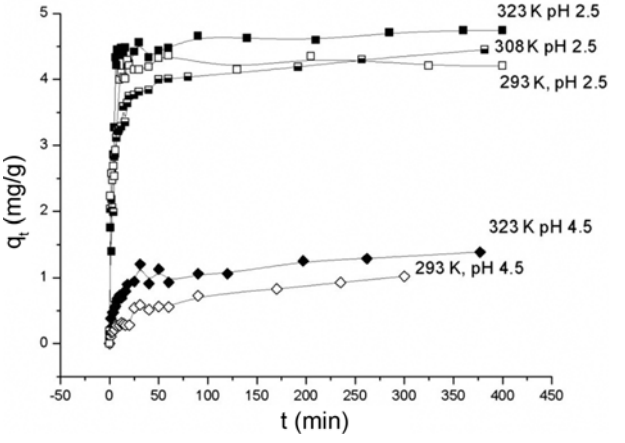

Figure 13. Kinetic adsorption isotherms of PET-NCPCL fibers as function of the pH and the temperature.

$$\frac{dq_t}{dt} = k_1(q_e - q_t) \quad (8)$$

integrated in the boundary conditions:

$$\ln(q_e - q_t) = \ln(q_e) - k_1 t \quad (9)$$

From the fit of $\ln(q_e - q_t)$ against t, k_1 and q_e can be obtained. However, if the intercept does not equal q_e, then the reaction is unlikely to be a first-order reaction even though the plot presents a high correlation coefficient with the experimental data.

The pseudo-second-order model is described with the following equation:

$$\frac{dq_t}{dt} = k_2(q_e - q_t)^2 \quad (10)$$

integrated in the boundary conditions:

$$\frac{t}{q_t} = \frac{1}{k_2 q_e^2} + \frac{1}{q_e} t \quad (11)$$

From the fit of t/q_t against t, k_2, and q_e can be obtained. The values of q_t and q_e are the amount adsorbed at time t and the equilibrium (mg/g), respectively. k_1 (min^{-1}) and k_2 (g/mg·min) are the equilibrium rate constants of the first-order and second-order models, respectively.

Many research studies have reported that the adsorption of dyes from solution follows the pseudo-second-order model [46-49]. The kinetic results presented in Figure 10 and 11 have been fitted to the pseudo-first-order and pseudo-second-order models, respectively, but they fit only the pseudo-second-order model significantly. This equation is based on the sorption capacity of the solid phase, and In contrast to other models, it predicts the behavior of the systems, in which the chemical exchange could be the controlling step. In our opinion, it can be applied to explain the interaction between the positively charged fiber surface and the anionic groups of GO.

Table 4. Kinetic parameters of adsorption fits to pseudo-second-order model

Kinetic constants	323K		293 K	
	pH 2.5	pH 4.5	pH 2.5	pH 4.5
PA 66-GO (C_i 50 mg/*l*)				
$q_{e,exp}$ (mg/g)	5.92	2.97	2.28	0.77
$q_{e,mod}$ (mg/g)	6.06	3.01	1.01	0.81
k_2 (g/mg·min)	0.0093	0.015	0.063	0.021
$t_{1/2}$ (min)	74.8	47.2	11.1	32.7
R^2	0.999	0.997	1	0.991
PET-NCPCI-GO (C_i 50 mg/*l*)				
$q_{e,exp}$ (mg/g)	4.74	1.391	4.204	1.02
$q_{e,mod}$ (mg/g)	4.75	1.299	4.234	1.05
k_2 (g/mg·min)	0.106	0.075	0.284	0.032
$t_{1/2}$ (min)	6.5	9.2	2.5	21.9
R^2	0.988	0.999	0.999	0.968

In Table 4, the values of the constants of these fits for both fibers are presented. The values of the amount adsorbed at the equilibrium, q_e, obtained experimentally and derived from the model are quite similar, as required [48]. When the kinetic data at 323 K and 293 K are compared, it can be observed that the process for PET-NCPCl is faster than that for PA 66. For PET-NCPCl, it is observed that the values at the equilibrium depend only on the pH and they remain constant with temperature. Similar results were observed with tannic acid on leacril [50] and chlorhexidine on cellulosic fibers [51].

When the adsorbent is PA 66, the process is slower, with half time values, $t_{1/2}$, being more than ten times higher than those for the PET fibers, possibly because the amount adsorbed is higher, and different interaction mechanisms are involved in the process. The combination of the Freundlich adsorption model and the pseudo-second-order kinetic model has been observed by several researchers working with GO as a composite adsorbent for systems such as chitosan/GO and MHC/GO (magnetic hydroxypropyl chitosan) for metals [48,49].

Desorption Experiments

An experimental test carried out at room temperature in two solutions, 10^{-3} M KCl and deionized water, for a contact time of 48 h was performed to verify that the amount of GO adsorbed onto the fibers remains constant. The spectroscopic measurements show that no desorption of GO could be observed under the chosen conditions.

Adsorption of Cationic Dyes onto the PA 66-GO Fibers

The suitability of PA 66-GO fibers in removing two different cationic dyes, crystal violet (CV) and Rhodamine B (RB), and a reactive dye Remazol Brillant Blue R (RBBR) from aqueous solutions was evaluated by kinetic experiments carried out under natural conditions, 295 K and a value of pH of water dye solutions. The PA 66-GO fibers were pre-treated in the best adsorption conditions, which are an initial concentration of the GO emulsion of 75 mg/*l*, pH 2.5, and 323 K. The initial concentration of the treatment has been adjusted at the higher absorbance of the dye under the Lambert Beer law, close to 1. The experimental conditions for each dye are as follows:

a) Cristal Violet. Molecular weight, 407.99 g/mol; initial concentration, 5 mg/*l* and initial adsorbance, 1.0024; pH 6.75; maximum wavelength, 590 nm; half adsorption time, $t_{1/2}$, is 2 min and 0.7 min for the untreated PA 66 fibers and PA 66-GO, respectively.

b) Rhodamine B. Molecular weight, 479.024 g/mol; initial concentration, 5 mg/*l* and initial absorbance, 0.801; pH 6.12;

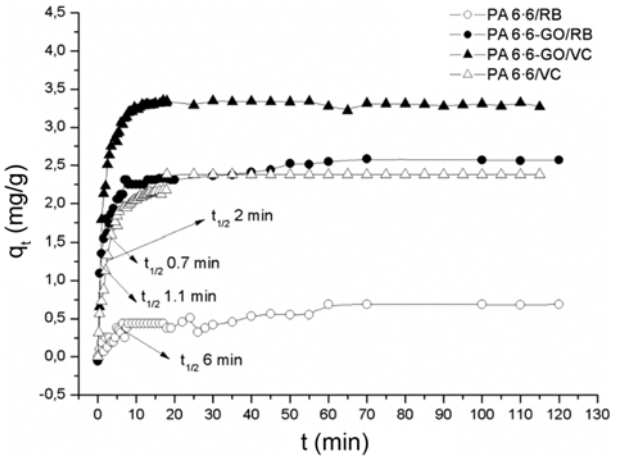

Figure 14. Kinetic adsorption isotherms Cristal Violet (CV) and Rhodamine B (RB) on untreated PA 66 and PA 66-GO fibers at 285 K and natural pH.

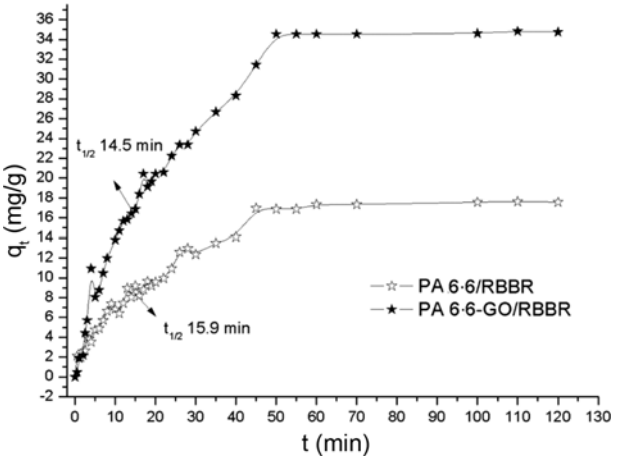

Figure 15. Kinetic adsorption isotherms of Remazol Brillant Blue R (RBBR) on untreated PA 66 and PA 66-GO fibers at 285 K and natural pH.

maximum wavelength, 535 nm; half adsorption time, $t_{1/2}$, is 6 min and 1.1 min for the untreated PA 66 fibers and PA 66-GO, respectively.

c) Remazol Brillant Blue R(RBBR): molecular weight, 626.55 g/mol; initial concentration, 75 mg/*l* and initial absorbance, 0.9652; pH 6.09; maximum wavelength, 593 nm; half adsorption time, $t_{1/2}$, is 15.9 min and 14.5 min for the untreated PA 66 fibers and PA6.6-GO, respectively.

The electrokinetic and thermodynamic characteristics of the adsorption of these dyes on different fibers have been previously studied in our laboratory [52,53]. The results of the amount of dye adsorbed versus time are presented in Figure 14 for the two cationic dyes and in Figure 15 for the reactive dye. It can be observed that all the dyes tested show a positive contribution of the coated GO in the process of the adsorption of dyes under these natural conditions, as well as a bigger rate of adsorption. Therefore, the previous coverage of polyamide fibers would improve the elimination of dyes from water. Dyed fiber samples were then washed, and no desorption of the dye from PA 66-GO was observed.

Conclusion

The results presented in this study show that the adsorption of GO on the two synthetic fibers, PA 66 and PET-NCPCl, is favored if the pH of the solution is lower than the isoelectric point of the fibers. In such a situation, the fibers present a positive zeta potential, and as the GO particles exhibit a negative charge in the range of the pH tested, 2-10 pH units, the interaction should be first attributed to electrostatic forces. The structural characterization data obtained by both SEM and Raman spectroscopy point to different mechanisms of the adsorption process. While the GO sheets appear to envelop the polymer of PA, suggesting a certain uniformity in the coating of the fiber, possibly pointing to a monolayer coverage, the interaction with PET-NCPCl appears to be more irregular. Moreover, molecular clusters seem to be specially formed possibly because of the great heterogeneity of the fiber-NCPCl system with the GO particles forming agglomerated aggregates or lumps, thus resulting in a multilayer arrangement at the specific bonding places where the NCPCl molecules were previously linked.

The isotherm analysis for the two different fibers indicates that both systems are better described by the Freundlich model, suggesting that there are unspecific interactions on the heterogeneous surface, which are characteristics of the multilayer adsorption. Additionally, the kinetic data fit well to the pseudo-second-order model, implying that some sort of chemisorption should govern at least the first stage of the adsorption, corroborated by the positive values of DH obtained. Because of the combination of the Freundlich isotherm and pseudo-second-order kinetic models, several mechanisms of the interaction should be considered to explain the adsorption. It is possible that the first stage is governed mainly by electrostatic forces and favoured by temperature, and in the second stage of hydrogen bonding, acid-base interactions and van der Waals forces could be responsible for unspecific adsorbate-adsorbate interactions. On the other hand, there is no noticeable desorption of GO under ambient conditions, and therefore, the interaction between the fibers and GO could be considered sufficient to keep the system stable in water media. The comparative kinetic analysis of the adsorption capacity of PA 66 and PA 66-GO towards two cationic dyes, Cristal Violet and Rhodamine B, under natural conditions, 295 K and the pH of the solution between 6 and 7, shows that the coated GO favours the amount adsorbed and increases the rate of adsorption. The polyamide fibers have many advantages, including a high adsorption capacity towards GO under specific conditions, no need for pre-treatment of the

polymer, and a low manufacturing cost. In addition, the PA 66-GO fibers have a higher reactivity with different dyes and it is possible to remove and replace the fiber-GO system once it is saturated with residual dyes. Therefore, we consider that this combined adsorbent, PA 66-GO, could be useful to eliminate pollutant compounds from wastewater.

Acknowledgements

Universidad de Jaén has provided financial support, thanks to the project number UJA2015/06/13 in collaboration with the foundation Caja Rural de Jaén. We wish to express our gratitude to the Center for Scientific and Technical Instrumentation of Jaén University, for the assistant support in FESEM and RAMAN determinations.

References

1. A. B. Cundy, L. Hopkinson, and R. L. D. Whitby, *Sci. Total Environ.*, **400**, 1 (2008).
2. M. N. Chong, B. Jin, C. W. K. Chow, and C. Saint, *Water Res.,* **44**, 2997 (2010).
3. S. K. Dickin, C. J. Schuster-Wallace, M. Qadir, and K. Pizzacalla, *Environ. Health Perspect.*, **124**, 900 (2016).
4. K. Shankar, J. I. Basham, N. K. Allam, O. K. Varghese, G. K. Mor, X. Feng, and C. A. Grimes, *J. Phys. Chem. C*, **113**, 6327 (2009).
5. P. Yuan, M. Fan, D. Yang, H. He, D. Liu, A. Yuan, and T. Chen, *J. Hazard. Mater.*, **166**, 821 (2009).
6. G. Zelmanov and R. Semiat, *Water Res.,* **42**, 492 (2008).
7. R. Jain, V. K. Gupta, and S. Sikarwar, *J. Hazard. Mater.*, **182**, 749 (2010).
8. X. Yue, F. Jiang, D. Zhang, H. Lin, and Y. Chen, *Fiber. Polym.,* **18**, 2102 (2017).
9. H. Vojoudi, A. Badiei, A. Amiri, A. Banaei, G. M. Ziarani, and K. Schenk-Joß, *J. Phys. Chem. Solids*, **113**, 210 (2018).
10. M. M. Dubinin, *Carbon*, **27**, 457 (1989).
11. F. Caturla, M. Molina-Sabio, and F. Rodriguez-Reinoso, *Carbon*, **29**, 999 (1991).
12. M. Valix, W. H. Cheung, and G. McKay, *Chemosphere*, **56**, 493 (2004).
13. X. Dong, X. Zhao, L. Wang, and W. Huang, *Curr. Phys. Chem.*, **3**, 291 (2013).
14. M. J. John and S. Thomas, *Carbohydr. Polym.*, **71**, 343 (2008).
15. E. P. Randviir, D. A. Brownson, and C. E. Banks, *Mater. Today*, **17**, 426 (2014).
16. G. K. Ramesha, A. V. Kumara, H. B. Muralidhara, and S. Sampath, *J. Colloid Interface Sci.*, **361**, 270 (2011).
17. I. Duru, D. Ege, and A. R. Kamali, *J. Mater. Sci.*, **51**, 6097 (2016).
18. J. Zhao, Z. Wang, J. C. White, and B. Xing, *Environ. Sci. Technol.*, **48**, 9995 (2014).
19. P. Xu, G. M. Zeng, D. L. Huang, C. L. Feng, S. Hu, M. H. Zhao, and Z. F. Liu, *Sci. Total Environ.*, **424**, 1 (2012).
20. X. Zuo, S. He, D. Li, C. Peng, Q. Huang, S. Song, and C. Fan, *Langmuir*, **26**, 1936 (2009).
21. T. Hartono, S. Wang, Q. Ma, and Z. Zhu, *J. Colloid Interface Sci.,* **333**, 114 (2009).
22. W. Gao, M. Majumder, L. B. Alemany, T. N. Narayanan, M. A. Ibarra, B. K. Pradhan, and P. M. Ajayan, *ACS Appl. Mater. Interfaces*, **3**, 1821 (2011).
23. A. Di Pierro, G. Saracco, and A. Fina, *Comp. Mater. Sci.*, **142**, 255 (2018).
24. H. Zhang, J. Cao, W. Wu, Z. Cao, and H. Ma, *Cellulose*, **23**, 3761 (2016).
25. M. Tian, L. Qu, X. Zhang, K. Zhang, S. Zhu, X. Guo, and Y. Sun, *Carbohydr. Polym.*, **111**, 456 (2014).
26. D. Kowalczyk, W. Fortuniak, U. Mizerska, I. Kaminska, T. Makowski, S. Brzezinski, and E. Piorkowska, *Cellulose*, **24**, 4057 (2017).
27. S. Gomari, I. Ghasemi, and M. Esfandeh, *Fiber. Polym.*, **18**, 2153 (2017).
28. E. Forgacs, T. Cserhati, and G. Oros, *Environ. Int.*, **30**, 953 (2004).
29. G. Zhao, J. Li, X. Ren, C. Chen, and X. Wang, *Environ. Sci. Technol.,* **45**, 10454 (2011).
30. I. Chowdhury, M. C. Duch, N. D. Mansukhani, M. C. Hersam, and D. Bouchard, *Environ. Sci. Technol.*, **48**, 961 (2014).
31. I. E. M. Carpio, C. M. Santos, X. Wei, and D. F. Rodrigues, *Nanoscale*, **4**, 4746 (2012).
32. J. A. Moleon, A. Ontiveros-Ortega, E. Gimenez-Martin, and I. Plaza, *Dyes Pigm.*, **122**, 310 (2015).
33. H. J. Jacobasch, G. Bauböck, and J. Schurz, *Colloid Polym. Sci.,* **263**, 3 (1985).
34. M. Espinosa-Jiménez, R. Padilla-Weigand, A. Ontiveros-Ortega, M. M. Ramos-Tejada, and R. Perea-Carpio, *J. Colloid Interface Sci.*, **265**, 227 (2003).
35. F. T. Thema, M. J. Moloto, E. D. Dikio, and M. Khenfouch, *J. Chem.,* **2013**, Article ID 150536 (2013).
36. A. C. Ferrari, J. C. Meyer, V. Scardaci, C. Casiraghi, M. Lazzeri, F. Mauri, and A. K. Geim, *Phys. Rev. Lett.*, **97**, 187401 (2006).
37. I. Langmuir, *J. Am. Chem. Soc.,* **40**, 1361 (1918).
38. H. M. F. Freundlich, *J. Phys. Chem.*, **57**, 385 (1906).
39. R. Jain, V. K. Gupta, and S. Sikarwarm, *J. Hazard. Mater.*, **182**, 749 (2010).
40. A. Soleimani-Gorgani and J. A. Taylor, *Dyes Pigm.*, **68**, 109 (2006).
41. E. Giménez-Martín, M. López-Andrade, J. A. Moleón-Baca, M. A. López, and A. Ontiveros-Ortega, *JSEMAT*, **5**, 190 (2015).
42. G. Alberghina, M. Longo, and M. Torre, *Dyes Pigm.*, **4**, 49 (1983).
43. Y. Qi, M. Yang, W. Xu, S. He, and Y. Men, *J. Colloid Interface Sci.*, **486**, 84 (2017).
44. Y. S. Ho and G. McKay, *Process Saf. Environ. Prot.*, **76**,

183 (1998).
45. Y. S. Ho and G. McKay, *Process Biochem.,* **34**, 451 (1999).
46. A. S. Özcan and A. Özcan, *J. Colloid Interface. Sci.*, **276**, 39 (2004).
47. S. Wang, H. Sun, H. M. Ang, and M. O. Tadé, *Chem. Eng. J.*, **226**, 336 (2013).
48. Y. S. Ho and G. McKay, *Chem. Eng. J.*, **70**, 115 (1998).
49. Y. Wang, L. Shi, L. Gao, Q. Wei, L. Cui, L. Hu, and B. Du, *J. Colloid Interface Sci.,* **451**, 7 (2015).
50. E. Chibowski, M. Espinosa-Jiménez, A. Ontiveros-Ortega, and E. Giménez-Martin, *Langmuir*, **14**, 5237 (1998).
51. E. Giménez-Martín, M. López-Andrade, A. Ontiveros-Ortega, and M. Espinosa-Jiménez, *Cellulose*, **16**, 467 (2009).
52. E. Giménez-Martín and M. Espinosa-Jiménez, *Colloids Surf., A*, **270**, 93 (2005).
53. M. Espinosa-Jiménez, E. Giménez-Martin, and A. Ontiveros-Ortega, *Text. Res. J.*, **67**, 677 (1997).